# Switching by domain wall automotion in asymmetric ferromagnetic rings

**Mohamad-Assaad Mawass[1,2,3], Kornel Richter[1], Andre Bisig[1,2], Robert M. Reeve[1], Benjamin Krüger[1], Markus Weigand[2], Andrea Krone[1], Hermann Stoll[2], Florian Kronast[3], Gisela Schütz[2] and Mathias Kläui[1,4]**

[1]*Johannes Gutenberg Universität-Mainz, Institut of Physics, Staudinger Weg 7, 55128 Mainz, Germany*
[2]*Max Planck Institute for Intelligent Systems, Heisenbergstr. 3, 70569 Stuttgart, Germany*
[3]*Helmholtz-Zentrum Berlin für Materialien und Energie, Albert-Einstein-Str. 15, 12489 Berlin, Germany*
[4]*Graduate School of Excellence Materials Science in Mainz (MAINZ), Staudinger Weg 9, 55128 Mainz, Germany*

## Abstract

Spintronic applications based on magnetic domain wall (DW) motion, such as magnetic data storage, sensors and logic devices, require approaches to reliably manipulate the magnetization in nanowires. In this work, we report the direct dynamic experimental visualization of reliable switching from the onion to the vortex state by DW automotion at zero field in asymmetric ferromagnetic rings using a uniaxial field pulse. Employing time-resolved X-ray microscopy, we demonstrate that depending on the detailed spin structure of the DWs and the size and geometry of the rings, the automotive propagation can be tailored during the DW relaxation from the higher energy onion state to the energetically favored vortex state, where both DWs annihilate. Our measurements show DW automotion with an average velocity of about ~ 60 m/s, which is a significant speed for spintronic devices. Such motion is mostly governed by local forces resulting from the geometry variations in the device. A closer study of the annihilation process via micromagnetic simulations reveals that a new vortex is nucleated in-between the two initial walls. We demonstrate that the annihilation of DWs through automotion in our scheme always occurs with the detailed topological nature of the walls only influencing the DW dynamics on a local scale. The simulations show good quantitative agreement with our experimental results. These findings shed light on a robust and reliable switching process of the onion state in ferromagnetic rings, which paves the way for further optimization of these devices.

## I. Introduction:

Reliable switching of magnetic elements is a key prerequisite for their employment in devices such as magnetic memory [1 - 4]. The ring geometry has been identified as a particularly well-suited geometry, as the flux-closure vortex state is completely stray-field free [5] in contrast to a disc, for instance, where the vortex core can still generate a sizeable stray field. Thus the two-fold energetically degenerate vortex state in a ring has a particularly high stability and was shown to be present even in small structures [6]. In order to switch between the two possible vortex states used for data storage (clockwise and counterclockwise) directly, circular magnetic fields or similar complex fields would be needed, which are difficult to generate [7, 8]. A simpler and more accessible method is to switch with a homogeneous field from the "vortex state" to the "onion state" with two DWs [9 - 12] and then back to the vortex state with opposite sense of rotation. Using asymmetric rings, this can be achieved by applying a uniaxial magnetic field to generate the onion state and then the two DWs move due to the asymmetry of the ring as previously shown [13]. By engineering the ring asymmetry and the field direction, the two DWs can move towards each other and if they annihilate they form one of the vortex states. On reversing the applied field direction the opposite onion state is obtained and by symmetry arguments this then switches to the opposite vortex state. So fundamentally we can switch between two vortex states by going via the appropriate onion state and this means one can switch between the vortex states using just a uniaxial field with no need for complex circular fields. This was proposed theoretically [14] for tailored geometries with asymmetries and experimentally it was shown that switching in asymmetric rings can lead to a desired vortex chirality [15].

However, so far only the static switched states have been investigated [16] and the dynamics and the time scale for the switching are not knowns. Furthermore, the switching from the onion to the vortex state needs to occur without any additional external fields if one wants to operate the device with a single field direction, which is desirable for simple device design. This requires DW automotion driven by the internal forces resulting from the device geometry and the accompanying spin structure changes [17]. This automotion process is so far little explored, but has been theoretically proposed for spintronics interconnects [18]. Experimentally the details of the automotion are not known and in particular the speed and reliability needs to be determined in order to gauge the applicability for devices. Furthermore, since DWs are predicted to be attracted to each other or repelled from each other, depending on their topology [19], it is unclear for instance how the repulsion prevents one from using the automotion to switch into the vortex state where the DWs need to be fully annihilated.

Consequently in order to develop devices with switching by DW automotion, the dynamics of this special process need to be understood and controlled and the robustness of the switching process needs to be ascertained.

In this paper, we study DW automotion, when two DWs propagate towards each other, without an externally applied field. We show that such motion in ferromagnetic rings is mostly governed by local forces. Through a closer look at the annihilation process using micromagnetic simulations we

reveal the details of how the process occurs. We explain our data based on three dynamical forces that drive the DW. The observation of the DW automotion and annihilation process sheds light on the switching of the onion state in ferromagnetic rings, which paves the way for further optimization of these devices.

## II.    Samples and experimental

Asymmetric ferromagnetic permalloy rings were fabricated with an outer diameter of 5.5 µm and non-centered inner diameter of 4 µm, and a thickness of 30 nm (Fig. 1). Variation of the DW potential landscape was introduced to the sample by this non-concentric geometry. Here the inner circular cut-off is shifted with respect to the outer circular edge of the ring, making the width of the ring angularly dependent (Figure 1(a)) [13]. For the experiment the ferromagnetic rings are initialized in the onion state [16], following a magnetic field excitation pulse. Afterwards the magnetic structure is relaxed and the domain and DW dynamics are observed at zero external field. In particular, automotive DW propagation driven by the gradient in energy resulting from the varying width leads to the lowest energy state (vortex state) being attained on a time scale of a few tens of nanoseconds.
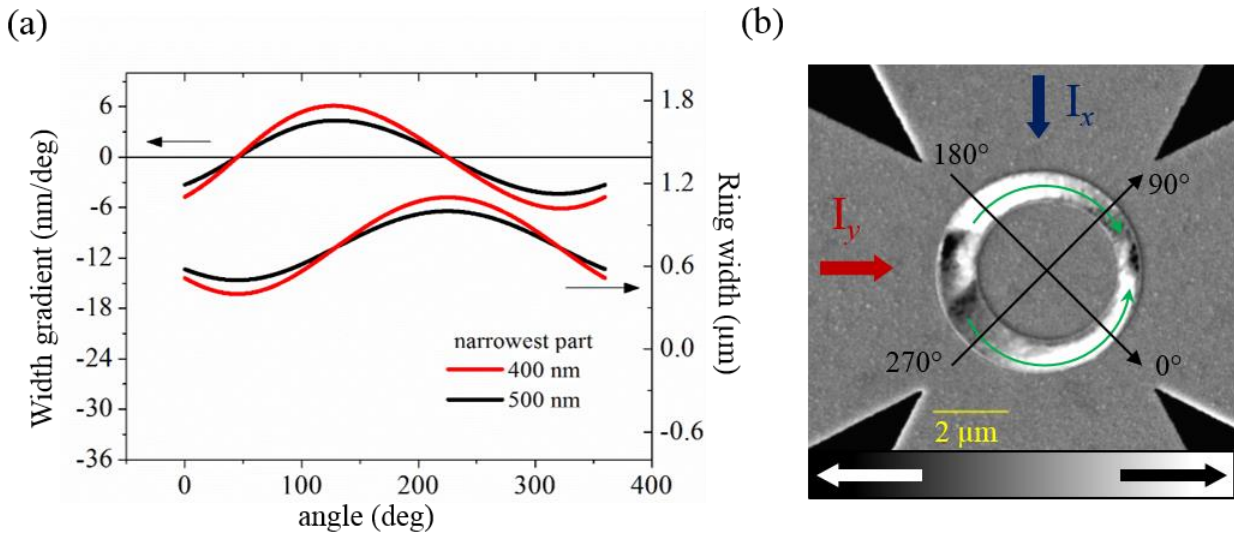


**Figure 1: Schematic of the sample geometry and layout used in the experiment. (a)** Angular variation of the sample geometry for different rings with narrowest widths of 400 and 500 nanometers. **(b)** Merged STXM-XMCD image of an asymmetric ring in the onion state with a scanning electron micrograph image of the sample under investigation. The unidirectional in-plane magnetic field pulse is generated by burst current pulses, $I_{x,y}$, injected through one or both crossed-striplines, depending on the desired magnetic field orientation. Black (white) contrast corresponds to magnetization pointing to the left (right), as illustrated by the green arrows and the greyscale bar is provided.

The time evolution of the magnetization dynamics is recorded stroboscopically via a pump and probe technique employing time resolved scanning transmission X-ray microscopy (STXM), with a sub 30 nm spatial resolution, at the MAXYMUS endstation of the BESSY II synchrotron [20, 21]. The in-plane magnetization component was imaged by tilting the sample surface normal by 30° with respect to the incident light direction. The contrast of the image is based on the X-ray magnetic circular dichroism (XMCD) effect [22]. The data were recorded at the Ni L₃-absorption edge (852.7 eV). In this study, the pump process consists of a short unidirectional or rotating in-plane magnetic field pulse.

Thus, the excitation signal can be either one of the two following cases: Firstly, a burst current pulse, $I_{x,y}$, injected through one or both crossed-striplines, depending on the desired magnetic field orientation leading to an unidirectional field pulse. Secondly rotating magnetic field pulses created by injecting two continuous sinusoidal signals, 90° phase shifted, which pass simultaneously through the two ends of crossed striplines (figure 1(b)) and are then switched off to initialize the onion state along a desired direction.

The maximum pulse amplitude used in this experiment for the rotating magnetic field pulse was $5\,V$, whereas $7\,V$ was used for the unidirectional field pulse. These values correspond to a maximum current density of between $j \approx 10^{11}\,A/m^2$ and $j \approx 10^{12}\,A/m^2$, depending on the resistances of the samples used. This is roughly the limit before irreversible structural damage of our samples occurs due to heating. In order to minimize such damage we performed the measurement, with a Helium atmosphere in the microscope chamber and using pulses with a duty cycle of less than 25 %.

It is worth emphasizing that the experiment is repeated at a repetition rate of 832 kHz and the transmission X-ray signal is recorded over more than ten billion subsequent pulse cycles, and hence DW propagation events, ensuring a high signal-to-noise ratio and therefore visible contrast demonstrates the reproducibility and the reliability of our measurement results. Further details on the sample fabrication and experimental setup and measurement procedure can be found in Refs. [23, 24].

## III.    Results

As a first step, we record the magnetic structure after the injection of a short unidirectional uniform magnetic field excitation with field strength of **B** ≈ 9 mT and pulse duration of ~ 25 ns with a symmetric rise and fall-time which is approximately ~ 8 ns. The Zeeman energy is minimal when both DWs align with the applied in-plane external magnetic field. Thus the two DWs are roughly oriented along the axis of the field pulse, which is in this case the direction perpendicular to the symmetrical axis of the ring (i.e. 45° axis), as shown in figure 2(a). This figure depicts the initial magnetic configuration and position of the two DWs, for a 500 nm minimal width asymmetrical ring structure. In this case, we can clearly see two vortex DWs are present. The chirality of the two DWs is clockwise after a unidirectional magnetic field excitation. This is in contrast to the chirality that we find after a clockwise rotating magnetic field excitation with field strength of **B** ≈ 7 mT and pulse duration of ~ 100 ns. The latter consists of one full rotation with a constant field strength

**B**, and fixed rotation frequency, $f = 10\ MHz$, with a starting angle along the 45° axis direction, as shown in figure 2(b). Note that the azimuthal symmetric axis of the ring is along the 135° axis.

Here the two diametrically opposed vortex DWs have opposite chiralities after rotation [23, 24], as shown in figure 2(d). Note that the chirality of the nucleated DWs depend on the details of the nucleation process [25]. However, it is important to note that the chirality is reproducible, as seen from the strong contrast in Fig. 2(a,d).

In the next step, after the onion state nucleation process is finished and the magnetic field pulse is off, we dynamically image the spontaneous DW propagation for zero external applied fields.
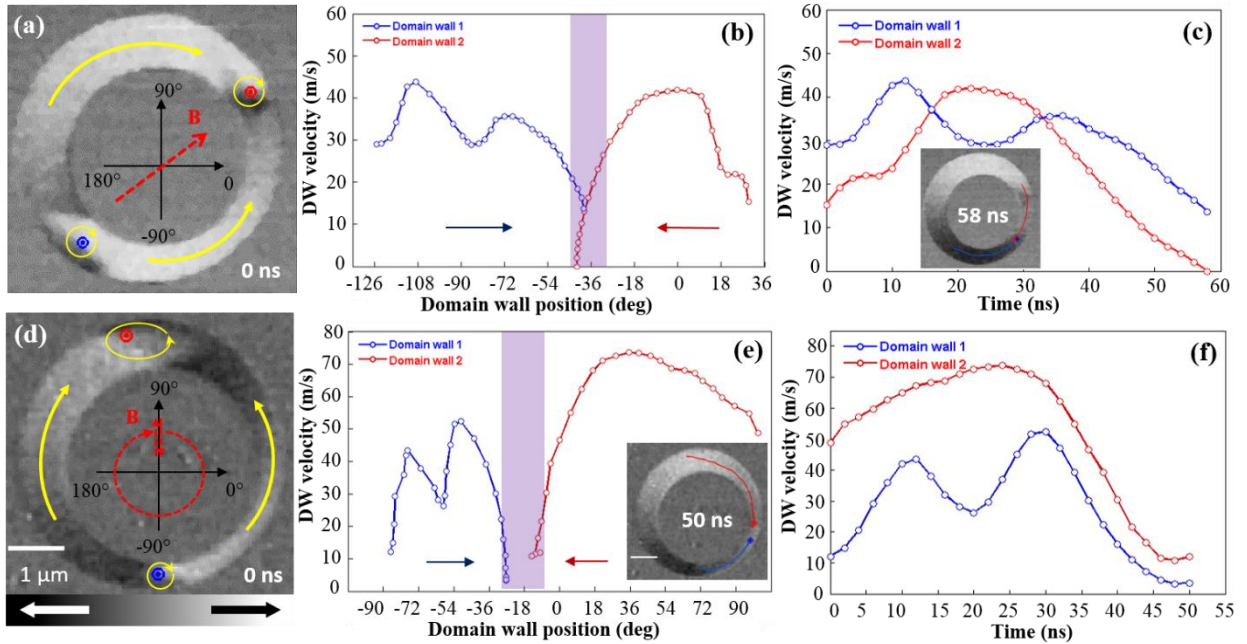


**Figure 2: Automotive DW propagation in an asymmetric ring: (a)** and **(d)** time-resolved XMCD-STXM images (at t = 0 ns) showing the relaxed onion state after excitation with a uniform external magnetic field, **B**, with direction indicated by the red arrow, either unidirectional **(a)** or rotational **(d)**, for the case of equal and opposite vortex wall chirality (500 and 400 nm minimum width), respectively. These images visualize the magnetization state just before the start of the automotion process. The vortex core polarity of both vortex walls is indicated in red (head-to-head) and blue (tail-to-tail). The yellow arrows indicate the direction of the magnetization. Panels **(b, c)** and **(e, f)** show the DW velocities (absolute values) plotted as a function of the azimuthal angle and time for the automotive propagation of two vortex walls with the same and opposite chirality, respectively. Blue and red arrows indicate the propagation direction of the DWs. The averaged annihilation area where DWs getting close enough is indicated in purple. Insets in panels **(c)** and **(e)** present the time-resolved XMCD-STXM snapshots at t = 58 ns and t = 50 ns showing the vortex state (clockwise) after the annihilation process of the DWs for the approach of two vortex walls with same and opposite chirality, respectively. Red and blue lines illustrate the trajectory of the DW vortex core, extracted from the time resolved movie. White (black) contrast corresponds to magnetization pointing to the right (left).

A snapshot of the moving DWs is taken every 2 ns, in a stroboscopic scheme as described above and detailed in Ref. [24]. Thus, these snapshots of the dynamic magnetic contrast represent time-resolved XMCD-STXM images. The temporal resolution of a single frame is limited by the electronics jitter to ~ 300 ps.

The vortex core positions are determined for each image from the black−white contrast manually. The instantaneous DW velocity is then calculated by applying a moving average filter as described in Ref. [24].

The results of the automotive DW propagation of two walls in the asymmetric ring, are shown in figure 2. Firstly, we consider the approach of two vortex walls having the same chirality, shown in figure 2(a-c). Here, the DWs start to move immediately after the magnetic field pulse is removed. The absolute velocity profiles (speed as a non-vectorial quantity) are given in figure 2(b, c) and show that the tail-to-tail wall (in blue) accelerates first and reaches as its maximum velocity after ~ 10 ns, whereas the maximum velocity of the head-to-head wall (in red) is reached later at ~ 25 ns. This can be easily explained by the fact that the initial position of the tail-to-tail DW is slightly closer to the highest width gradient of the ring than the head-to-head wall, since the onion state is not perfectly aligned with the perpendicular direction of the symmetrical axis of the asymmetric ring. Thus, the influence of shape of the sample on the DW resulting from the highest width gradient is highest at the beginning for the tail-to-tail wall.
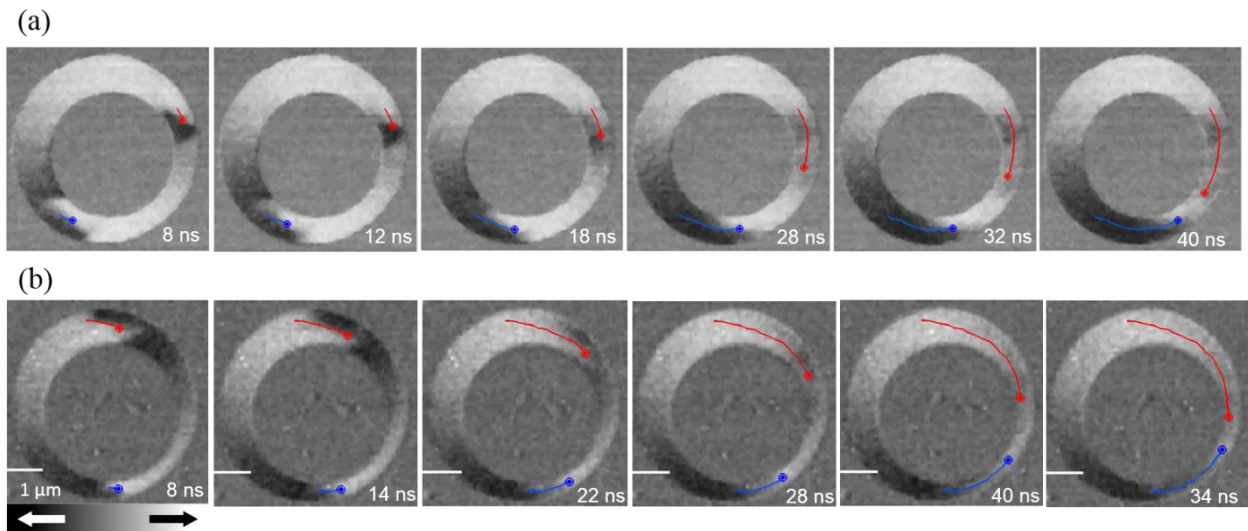


**Figure 3:** Time-resolved STXM-XMCD snapshots of automotive DWs motion during the switching process from the onion to the vortex state in the ferromagnetic rings, for the case of equal **(a)** and opposite **(b)** vortex wall chirality. These snapshots represent part of the XMCD movies used to extract the DW velocities plotted in figure 2. Red and blue lines illustrate the averaged trajectory of the vortex core of both vortex walls head-to-head and tail-to-tail, respectively.

The velocity of this wall oscillates slightly during the propagation, possibly due to a naturally occurring pinning center due to unavoidable defects and edge roughness from the fabrication process. The second increase in velocity for the tail-to-tail wall is smaller than for the first acceleration since the wall has already passed the highest width gradient position (see figure 1(a)), and is now closer to the narrowest part (zero width gradient) where both DWs annihilate. On the other side, the velocity of the head-to-head DW starts to decrease. We note that the global maximum velocity of both DWs during automotion is similar and sizeable (> 40 m/s).

In order to investigate the automotive vortex DW dynamics in relation to the topological character of the walls (chirality), we now study the approach of two vortex walls of opposite chirality as shown in figure 2(d-f). It can be seen that the velocity profile looks qualitatively similar to the previous one, however clear quantitative differences are apparent. In particular during the final stages of the DW approach. For instance, considering the tail-to-tail wall velocity plotted in blue in the graph of figure 2(b, c), we can see that the second peak in velocity is lower than the first one, whereas in figure 2(e, f) the second peak in velocity of the same wall is higher. Furthermore when comparing the time between these two local peak velocities and the full annihilation of the walls, we find that in the second case the annihilation occurs much sooner (~ 14 ns) than the first case (~ 24 ns).

It is worth mentioning that the details of the motion are influenced by the local structure of the device. Furthermore, the detailed DW spin structure is influenced by the device geometry and crystalline structure of the material that leads to possible local variations of the magnetic properties. Thus the exact details of the DW dynamics vary from one device to another and depend on the wall position. However the overall behavior of the motion of the DWs towards the narrow part of the ring is robust and has been observed in dozens of studied samples (not shown).

Moreover, we note that as known for all spontaneous and switching mechanisms, the exact evolution depends mainly on the pinning and thermal activation [26] which determine the time for reversal and modifies the evolution, leading to some blurring of the XMCD-image that is averaged across all repetitions in our experimental imaging technique, as described above (see figure 3). Therefore during the annihilation process, the image contrast of the vortex DWs is slightly blurred, leading to less accuracy in defining the exact vortex core position during the automotion and in particular when DWs enter the purple area where they annihilate, as shown in figure 2(b, e). In other words, the extracted DW position represents the averaged DW position which lead to a very small accuracy in defining the wall position in this area. This would explain the different behaviors observed correlated to the DW positions in the purple area in both cases (shown in figure 2(b, e)). These differences have no importance or physical meaning even though the topology of DWs is found to be important for the dynamics at this region. For example in one case (Fig. 2(b)) the red wall moves further to the left than the blue wall and in the other case (Fig. 2(e)) the walls do not even meet. This highlights the necessity to perform micromagnetic simulations which allow us to investigate the detailed intrinsic spin structure changes and their contribution to the DW dynamics in these regions.
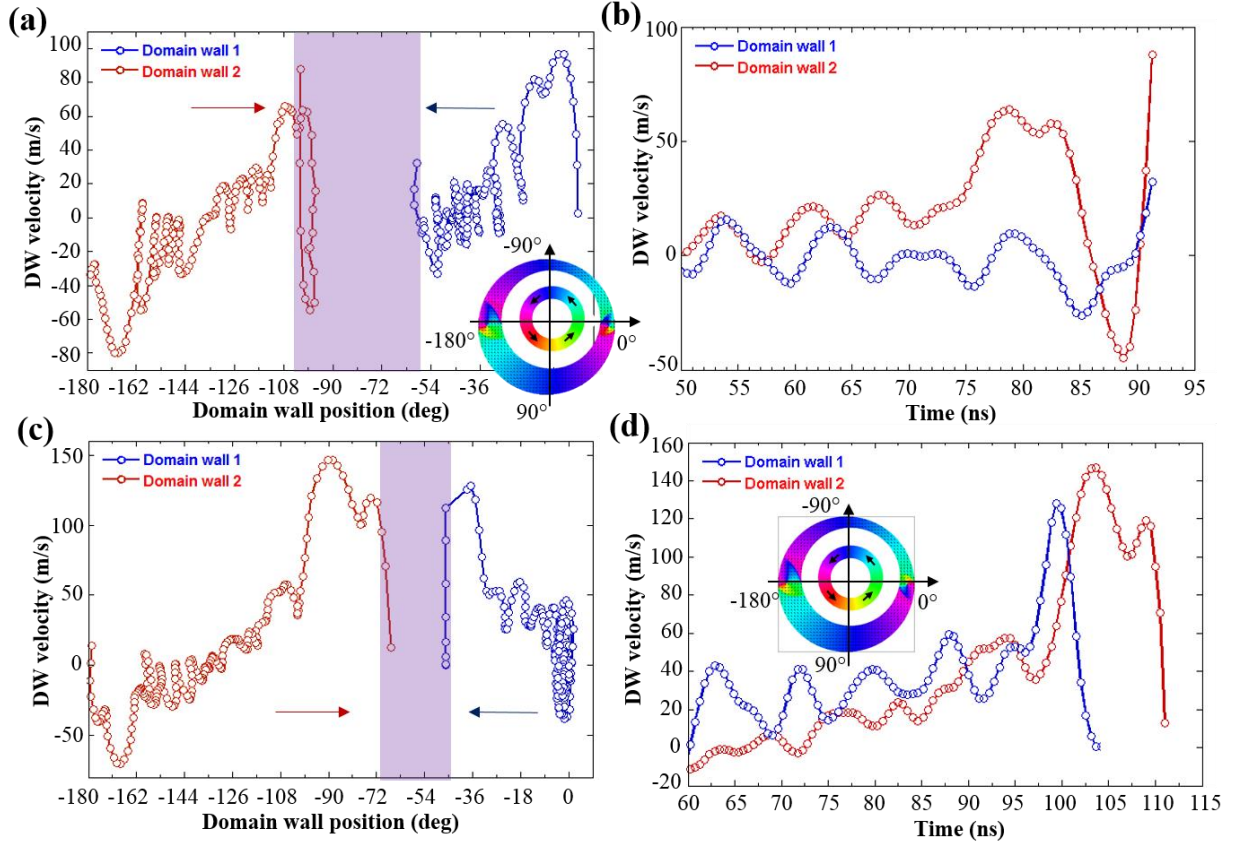
**Figure 4:** Micromagnetic simulations of DW dynamics at zero-field, comparing the velocity profiles of two different magnetic configurations where the DWs have the same (**Top**) and opposite chiralities (**Bottom**). Panels (**a, b**) and (**c, d**) show the DW velocities plotted as a function of the azimuthal angle and time for the automotive propagation of two vortex walls with the same and opposite chirality, respectively. The averaged annihilation area where DWs getting close enough is indicated in purple. Blue and red arrows indicate the propagation direction of the DWs. **Insets** in (**a**) and (**d**) show the spin structure of the 400 nm ring geometry for both cases with the head-to-head wall on the left and tail-to-tail wall on the right.

Thus, in order to understand the automotion in more detail and how these different behaviors relate to the topological nature of the walls we carried out micromagnetic simulations for the two cases of equal and opposite DW chirality. The micromagnetic simulation was performed using the MicroMagnum code [27]. The dimensions of the simulated asymmetric rings presented here are the same as those used in the experiment (figure 2(b)). The materials parameters used are the typical values for permalloy [23]: exchange stiffness $A = 1.3 \times 10^{-11} \, J/m$, saturation magnetization $M_s = 800 \times 10^3 \, A/m$, damping parameter $\alpha = 0.008$, no anisotropy and the cell size of $5 \times 5 \times 30 \, nm^3$. The position of the vortex core was determined by fitting a Gaussian through the $M_z$ component of the magnetization [24].

Figure 4 presents the micromagnetic simulations of DW dynamics at zero-field for different DW spin configurations. In figure 4(a, b), the DWs have the same polarity and same chirality, mirroring the experimental situation shown in figure 2(a-c) whereas in figure 4(c, d), the DWs have the same polarities and opposite chiralities, mirroring the experimental approach of two vortex wall of opposite chirality shown in figure 2(d-f). Thus by comparing both experimental (figure 2(e, f)) and simulated (figure 4(c, d)) results, we can see that the DW automotion seen in the micromagnetic simulations is in good qualitative agreement with the obtained experimental results. In particular the results shown in figure 4(c, d) reveal that the walls experience a strong attractive interaction once they get very close to each other, as observed also in the experiment. This effect manifests itself as a dramatic increase of the DW velocity just before the annihilation process occurs in the narrowest part of the ring whereas for the equal chirality case (figure 4(a, b)) such a large increase in the velocity is not seen in either the simulations or experiment. This is due to the attractive nature of the short-range exchange interaction force in the case of the opposite chirality resulting of the detailed topological nature of the walls. In the case of equal chirality walls this interaction force is repulsive [28].
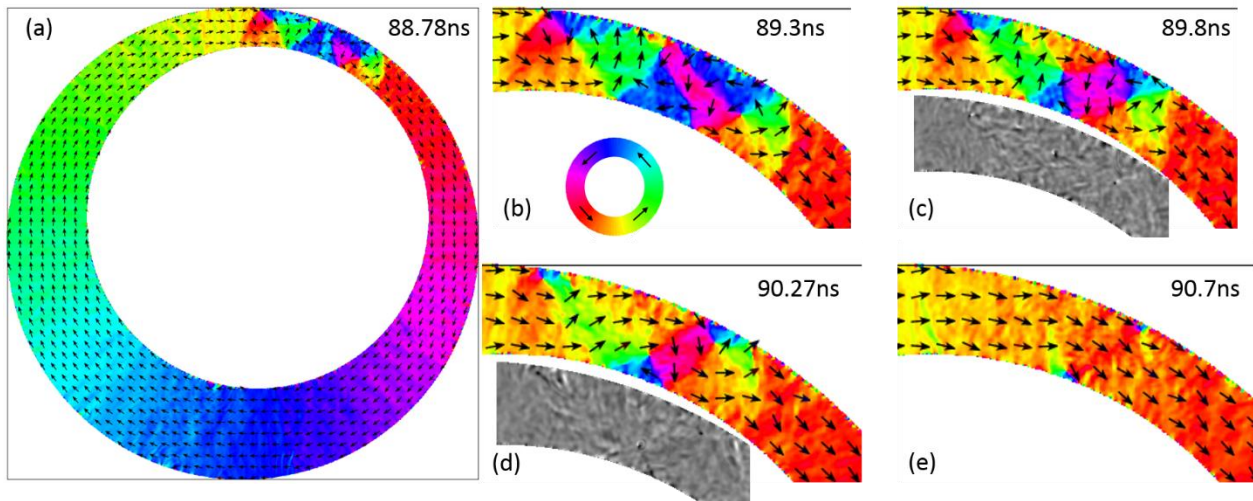


**Figure 5:** Micromagnetic simulations for the dynamic vortex DW spin structures during the annihilation process, where DWs have initially the same chiralities and polarities. (**a - e**) snapshots illustrating the last 2ns before the full annihilation of the DWs. Insets in (**c, d**) show the gray scale of the corresponding snapshots which represent the out-of-plane magnetization component ($M_z$) along the Z-direction, where white (black) indicates magnetization pointing up (down). The color code represent the in-plane magnetization direction visualized by the small black arrows.

On the other hand, many more oscillations of the velocity than in the experiment are seen in the micromagnetic simulation results (figure 4). This can be explained due to the fact that in our simulation the initial applied field is abruptly removed and hence the non-equilibrium spin structure

that leads then leads to velocity change (i.e. vortex core) move between the edge of the ring and the center-like. Furthermore, one cannot see a tight correlation between the initial wall topologies and the observed DW velocity profiles for large distances. This highlights that the topological interaction is important only for small distances between the DWs. Thus, next we focus on the annihilation process, where the topology of DWs is found to be important for the dynamics.

We note that when comparing figures 2(c) and 4(c) one needs to take into account significant differences. Indeed Fig. 2(c) is an average of 10 billion repetitions while Fig. 4(c) is a single simulation at T = 0. This means Fig. 2(c) shows only the reproducible parts of the displacement. From the contrast we can ascertain that the motion is largely reproducible. However the very fine structure in Fig. 4(c) showing very fast oscillations of the DW velocity will depend strongly on thermal excitations and details of the exact nanoscale DW spin structure. In the experiment these will be invariably washed out due to the averaging process as well as the thermal excitations. However the general trend, namely that the velocities first go up and then go down as the two walls approach is a key feature which is reproduced by the simulations.

Figure 5 shows micromagnetic simulation for the annihilation process of two vortex DWs having the same chirality. For this case, the closest edge defects between the two walls are along the same edge (inner-edge) of the nanowire [28]. In this figure we show the time resolved snapshot of annihilation process starting from t = 88.78 ns, which is roughly 2.6 ns before the full magnetization switching of the ring, from its initial onion state to the vortex state. We can see in figure 5(c) that at $t = 89.80\ ns$ a new vortex DW is nucleated in between the two initial vortex walls and this new wall has an opposite chirality to the initial walls. This nucleation phenomena is further illustrated in the insets of Figure 5(c, d) where the out-of-plane magnetization component ($M_z$) is plotted, where white (black) indicates magnetization pointing up (down). The arrows in the two-dimensional schemes represent the in-plane magnetization components. In the next steps (figure 5(d, e)) the two initial walls annihilate by being expelled from the same edge (outer-edge) of the nanowire, whereas the new vortex wall moves down and is expelled later (at $t = 91.30\ ns$ not shown).

Now, we compare this result to the annihilation process for the case of the vortex walls with opposite chiralities, presented in figure 6, where the closest edge defects are on opposite edges of the ring. Here, the annihilation process starts by annihilation of both adjacent edge defects located on the outer and inner ring edge followed by the nucleation of a new vortex core and antivortex core pair at $t = 109\ ns$ as shown, in detail, in Fig. 6(c, d). It is worth mentioning that the nucleated vortex DW has the same chirality as the left initial wall. Therefore, both walls experience a repulsive force due to their topology (same chirality) with the new vortex wall slightly pushed toward the outer ring edge as seen in (Fig. 6(d, e)). Afterwards in the next two subsequent snapshots (figure 6(e, f)) both walls annihilate by being expelled from the same ring edge (outer-edge) (similar to the previous case since both walls exhibit the same chirality), whereas the second initial vortex wall with opposite chirality is expelled just before from the opposite edge (inner-edge).
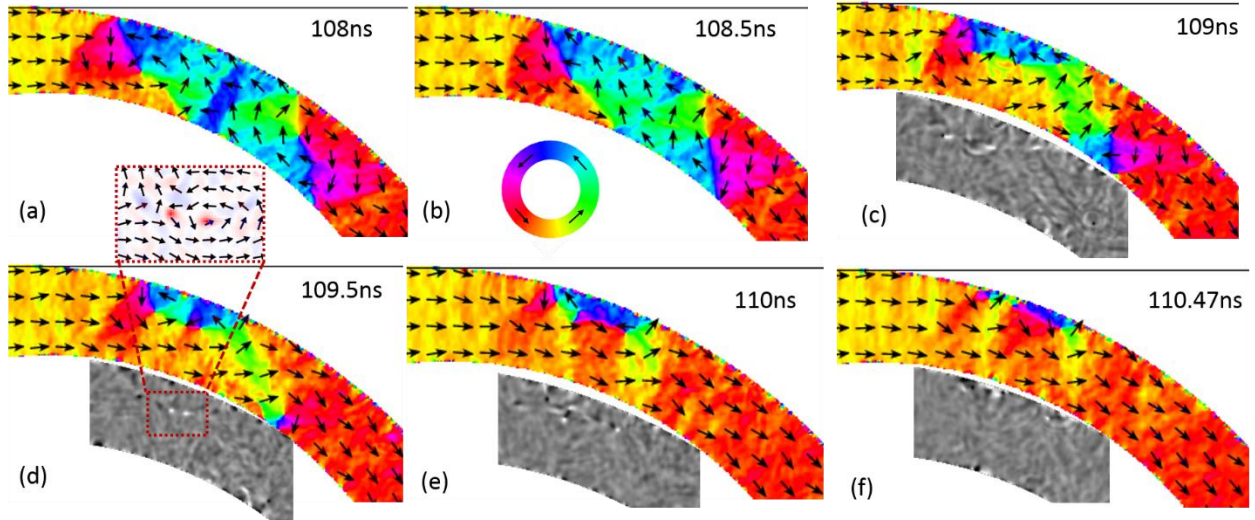
**Figure 6:** Micromagnetic simulation of the dynamic vortex DW annihilation process, where DWs have initially opposite chiralities and the same polarity. (**a - e**) panels illustrate the last 6 snapshots before the full annihilation of the DWs. The color code represents the in-plane magnetization direction visualized by the small black arrows. Insets in (**c - f**) show the gray scale of the corresponding snapshots which represent the out-of-plane magnetization component ($M_z$), where white (black) indicates magnetization pointing up (down). The color scale, in the close-up inset in (**d**) top, indicates the out-of-plane magnetization component, red (blue) indicates magnetization pointing up (down).

## IV.    Discussion

Our first surprising experimental observation of DW automotion (with an averaged velocity of ~ 60 m/s), in which the wall inertia is able to overcome both the repulsive topological force between the walls with the same chirality [28] and the barrier potential resulting from the unavoidable sample imperfections that pin the wall, has not been previously observed. We explain the underlying mechanisms of this behavior by considering the forces that act on the vortex DW spin structure.

For the sake of simplicity, we treat the DW as exhibiting point-particle behavior, and, consequently we can describe it by one single coordinate (the vortex core position). There are four forces acting on the vortex DW, one of which is a radial restoring force and the other three are tangential forces, which act as azimuthal driving forces.

Firstly the long-range attractive interaction between the walls, at large separation, is purely magnetostatic and largely independent of the chiral character of the DWs. In nanowires, the DWs in the long distance limit can be considered as free magnetic monopoles carrying a single opposite magnetic charge, with adjacent walls (head-to-head and tail-to-tail DWs) always having opposite charges [28].

Thus, the two walls always experience an attractive force (similar to the Coulomb force), pushing the walls towards each another, as is clear from the electrostatic analogy [29]. The relevant energy is mainly determined by the magnetic charge of the DWs which serve as sources of stray fields. Moreover, the interaction between walls (through stray fields) has a dipolar nature with the energy decreasing monotonically when the walls start to move towards one another. Hence, the resulting force is inversely proportional to the separation [28].

The second force that acts on the DW is the force resulting from the asymmetrical shape of our ring structure. As mentioned above, this force results from the spatially inhomogeneous potential landscape of the DW energy (Fig. 1), in the asymmetric ring landscape with a minimum and maximum in the narrowest and the widest part, respectively. The DW potential landscape has a spatial dependence due to the exchange and dipolar energy variations in the DW spin structure and thus it depends on the local ring width. This is demonstrated in Figure 7, where we show the contribution to the DW energy at zero field in 500 nm asymmetric rings. At zero field the DW energy consists only of the sum of the exchange energy and dipolar energy (in zero magneto crystalline anisotropy permalloy). The energies are obtained from micromagnetic calculations, by mirroring the DW along the ring to different positions. We can infer from the graphs in figure 7(b) that the DWs' energies scale with the width of the structure, demonstrating that the potential landscape can be tailored by the geometry. This force is therefore classified as a local and short range-force, proportional to the width-gradient in the ring.
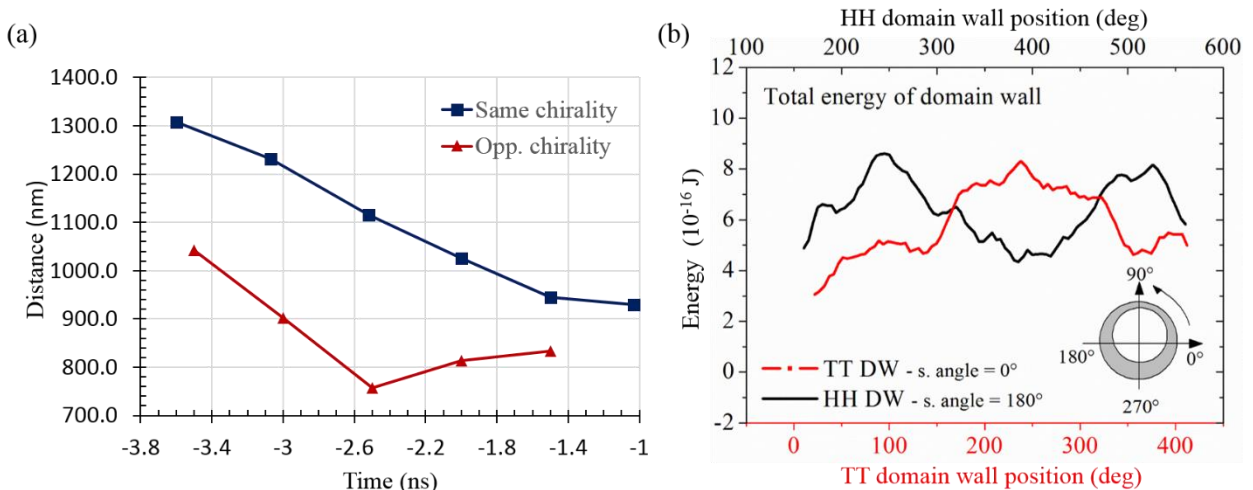


**Figure 7: (a)** Calculated distance between vortex cores plotted as a function of time (before the annihilation at t = 0 ns) for both studied cases in **Fig. 5** and **Fig. 6** where the vortex walls have same and opposite chirality, respectively. **(b)** Contributions to the DW energy at zero field (exchange + magnetostatic energies) in 500 nm asymmetric rings plotted as a function of DW position. The black and red curves correspond to the head-to-head (HH) and tail-to-tail (TT) vortex wall with a starting or initial angle at **0°** and **180°**, respectively. The energies are obtained from micromagnetic calculations, by propagating the DW along the ring with a field pointing along different directions.

The third force that acts on the DW is the force resulting from the short-range interactions, arising when the separation, d, between DWs become small. Contrary to the long-range attractive interaction force, this force depends on the detailed topological nature of the DWs (chirality) [28]. This leads to a repulsive or attractive interaction depending on whether the two vortex walls have the same or opposite chirality, respectively. This effect can be understood by considering the spin structure of the vortex walls, as discussed in Ref. [28]. For instance, in vortex DWs with the same chirality the spins between the two walls cannot continuously rotate, since the spins at both sides of the domain are anti-parallel. This leads to an increase of the exchange energy which opposes a further approach of both walls toward each another. In contrast for vortex walls carrying opposite chirality, the magnetization can rotate continuously since spins at both sides of the domain are parallel. Therefore these interaction forces are a consequence of topological edge defects.

Finally the radial force that acts on the vortex wall is the restoring force, resulting from the shape anisotropy, which pushes the vortex core toward the center of the nanowire and this depends on the radial vortex core position as well as the ring width and material.

Taking into account our experimental observations, we can conclude that automotive DW dynamics is mostly governed by the competition between local forces arising from the inhomogeneous potential landscape and the long-range interaction between walls for large distances ( $> 1$ μm). Since automotive DW motion always occurs toward the narrowest part of ring, we conclude that the long-range interaction between walls is smaller than the local forces from the inhomogeneous potential landscape. On the other hand, when two DWs approach each other, their mutual interaction becomes more important and this is governed by the topology of both DWs. This effect is revealed in figure 7(a) which presents the calculated distance between vortex cores plotted as a function of time for the two studied cases presented in figure 5 and figure 6, where the vortex walls have the same and opposite chirality, respectively. We can clearly infer from the graph that during the annihilation process the initial vortex DWs having the opposite chirality approach each other closer and faster than the case where the vortex DWs have the same chiralities. However, since we always observe annihilation and switching to the vortex state it is clear that the inertia of the walls is sufficient to overcome any barriers towards annihilation and thus robust switching is observed.

## V.    Conclusion

In summary, we have directly imaged DW automotion in asymmetric curved nanowires at zero field. We have demonstrated that automotive propagation occurs due to the influence of the demagnetization and exchange energy present in the structures. This automotion is driven by the interaction between the DWs spin structures, which depends on the topology of the system and by the energy gradient associated with the spin structure energy change when the geometry changes.

The pump and probe experiment of DW propagation at zero field revealed DW automotion with an average velocity of about ~ 60 m/s, which is a significant speed for spintronic devices based on

DW dynamics. We demonstrate that the DW inertia and the stored energy allows the walls to overcome both the local extrinsic pinning and the topological repulsion between DWs carrying the same winding number (vortex chirality), thus leading to robust switching from the onion to the vortex state.

Finally, we present a systematic micromagnetic simulation study of DW motion at zero-field in 400 nm asymmetric rings with the wall possessing different topological character. By performing a series of micromagnetic simulations on defect-free systems, we demonstrate that the DW automotion and annihilation is always present, and the results showed good quantitative agreement with our experimental results. Moreover we demonstrate that the detailed topological nature of the walls only influences the DW dynamics on a local scale without inhibiting the annihilation of DWs through automotion. These findings shed light on a robust and reliable switching process involving the onion state in ferromagnetic rings, which paves the way for further optimization of these devices. By increasing the width gradient of the system by modifying its geometry, consequently higher speeds of the switching process can be achieved.

## Acknowledgments

## References

[1] R. Waser and M. Aono, Nanoionics-based resistive switching memories, Nature Materials 6, 833 - 840 (2007).

[2] S. A. Wolf, D. D. Awschalom, R. A. Buhrman, J. M. Daughton, S. von Molnár, M. L. Roukes, A. Y. Chtchelkanova, D. M. Treger, Spintronics: A Spin-Based Electronics Vision for the Future, Science Vol. 294, Issue 5546, 1488 (2001).

[3] B. N. Engel, J. Akerman, B. Butcher, R. W. Dave, M. DeHerrera, M. Durlam, G. Grynkewich, J. Janesky, S. V. Pietambaram, N. D. Rizzo, J. M. Slaughter, K. Smith, J. J. Sun, S. Tehrani, A 4-Mb toggle MRAM based on a novel bit and switching method, IEEE Trans. Magn., vol. 41, no. 1, pp. 132 - 136 (2005).

[4] A. S. Mani, D. Geerpuram, A. Domanowski, V. Baskaran and V. Metlushko, Magnetic random access memory design using rings with controlled asymmetry, Nanotechnology 15, pp. S645-S648 (2004).

[5] J. Rothman, M. Kläui, L. Lopez-Diaz, C.A.F. Vaz, A. Beloch, J.A.C. Bland, Z. Cui, R. Speaks, Observation of a bi-domain state and nucleation free switching in mesoscopic ring magnets, Physical Review Letters 86, 1098 (2001).

[6] L. J. Heyderman, C. David, M. Kläui, C. A. F. Vaz and J. A. C. Bland, Nanoscale ferromagnetic rings fabricated by electron-beam lithography, J. Appl. Phys. 93, 10011 (2003).

[7] J. G. Zhu, Y. Zheng, G. A. Prinz. Ultrahigh density vertical magnetoresistive random access memory, Journal of Applied Physics, 87, 6668-6673 (2000).

[8] A. Imre, L. Zhou, A. Orlov, G. Csaba, G. H. Bernstein, W. Porod, V. Metlushko, Application of mesoscopic magnetic rings for logic devices, 4th IEEE Conference on Nanotechnology, pp. 137-139 (2004).

[9] M. Kläui, Head-to-head domain walls in magnetic nanostructures, Journal of Physics: Condensed Matter 20, 313001 (2008).

[10] S. McVietie, G. S. White, J. Scott, P. Warin, and J. N. Chapman. Quantitative imaging of magnetic domain walls in thin films using Lorentz and magnetic force microscopies. *J. Appl. Phys.* **90**, 5220 (2001).

[11] P. -O. Jubert, R. Allenspach, and A. Bischof. Magnetic domain walls in constrained geometries. *Phys. Rev. B* **69**, 220410 (2004).

[12] P. Bruno. Geometrically Constrained Magnetic Wall. *Phys. Rev. Lett.* **83**, 2425 (1999).

[13] K. Richter, A. Krone, M. -A. Mawass, B. Krüger, M. Weigand, H. Stoll, G. Schütz, and M. Kläui. Local Domain-Wall Velocity Engineering via Tailored Potential Landscapes in Ferromagnetic Rings. *Phys. Rev. Applied* **5**, 024007 (2016).

[14] S. Prosandeev, I. Ponomareva, I. Kornev, and L. Bellaiche, Control of Vortices by Homogeneous Fields in Asymmetric Ferroelectric and Ferromagnetic Rings, Phys. Rev. Lett. 100, 047201(2008).

[15] F. Q. Zhu, G. W. Chern, O. Tchernyshov, X.C. Zhu, J.G.Zhu and C. L. Cien, Magnetic bistability and controllable reversal of asymmetric ferromagnetic nanorings, Physical Review Letters 96, 027205 (2006).

[16] M. Kläui, C. A. F Vaz, L. Lopez-Diaz and J. A. C. Bland, Vortex formation in narrow ferromagnetic rings J. Phys.: Condens. Matter 15, R985 (2003).

[17] J. -Y. Chauleau, R. Weil, A. Thiaville, and J. Miltat. Magnetic domain walls displacement: Automotion versus spin-transfer torque. *Phys. Rev. B* **82**, 214414 (2010).

[18] D. E. Nikonov, S. Manupatruni, I. Young, Automotion of domain walls for spintronic interconnects, J. Appl. Phys. 115, 213902 (2014).

[19] E. -M. Hempe, M. Kläui, T. Kasama, D. Backes, F. Junginger, S. Krzyk, L. J. Heyderman, R. Dunin-Borkowski and U. Rüdiger. Domain walls, domain wall transformations and structural changes in permalloy nanowires when subjected to current pulses. phys .sat. sol. (a) 204, No. 12, 3922 – 3928 (2007).

[20] A. L. D. Kilcoyne et al. Interferometer-controlled scanning transmission x-ray microscopes at the advanced light source. Journal of Synchrotron Radiation, 10:125-136, (2003).

[21] H. Stoll, M. Noske, M. Weigand, K. Richter, B. Krüger, R. M. Reeve, M. Hänze, C. F. Adolf, F.-U. Stein, G. Meier, M. Kläui and G. Schütz. Imaging spin dynamics on the nanoscale using X-Ray microscopy. Front. Phys. 3, 26 (2015).

[22] G. Schütz, W. Wagner, W. Wilhelm, P. Kienle, R. Zeller, R. Frahm, and G. Materlik. Absorption of circularly polarized x rays in iron. Phys. Rev. Lett. 58, 737–740 (1987).

[23] A. Bisig, M. A. Mawass, M. Stärk, C. Moutafis, J. Rhensius, J. Heidler, S. Gliga, M. Weigand, T. Tyliszczak, B.V. Waeyenberge, H. Stoll, G. Schütz, M. Kläui. Dynamic domain wall chirality rectification by rotating magnetic fields. Appl. Phys. Lett. 106, 122401 (2015).

[24] A. Bisig, M. Stärk, M. -A. Mawass, C. Moutafis, J. Rhensius, J. Heidler, F. Büttner, M. Noske, M. Weigand, S.Eisebitt, T. Tyliszczak, B. V. Waeyenberge, H. Stoll, G. Schütz and M. Kläui. Correlation between spin structure oscillations and domain wall velocities. Nat. Commun 4, 2328 (2013).

[25] K. Richter, A. Krone, M. -A. Mawass, B. Krüger, M. Weigand, H. Stoll, G. Schütz, and M. Kläui. Localized domain wall nucleation dynamics in asymmetric ferromagnetic rings revealed by direct time-resolved magnetic imaging. Phys. Rev. B 94, 024435 (2016).

[26] M. Hayashi, L. Thomas, C. Rettner, R. Moriya, X. Jiang, and S. S. P. Parkin. Dependence of Current and Field Driven Depinning of Domain Walls on Their Structure and Chirality in Permalloy Nanowires. Phys. Rev. Lett. 97, 207205 (2006).

[27] http://micromagnum.informatik.uni-hamburg.de/

[28] L. Thomas, M. Hayashi, R. Moriya, C. Rettner and S. Parkin. Topological repulsion between domain walls in magnetic nanowires leading to the formation of bound states. Nat. Commun. 3, 810 (2012).

[29] O. Tchernyshyov and G. -W. Chern. Fractional vortices and composite domain walls in flat nanomagnets. Phys. Rev. Lett. 95, 197204 (2005).